JCTC Journal of Chemical Theory and Computation

Article

pubs.acs.org/JCTC

Multiscale Modeling Approach toward the Prediction of Viscoelastic Properties of Polymers

G. Maurel,[†,‡] B. Schnell,[†] F. Goujon,[‡] M. Couty,[†] and P. Malfreyt*[,‡]

[†]Manufacture Française des Pneumatiques MICHELIN, Centre de Ladoux, 23 place des Carmes, 63000 Clermont-Ferrand, France

[‡]Institut de Chimie de Clermont-Ferrand, ICCF, UMR CNRS 6296, Université Blaise Pascal, 63177 Aubière Cedex, France

ABSTRACT: We report a multiscale modeling approach to study static and dynamical properties of polymer melts at large time and length scales. We use a bottom-up approach consisting of deriving coarse-grained models from an atomistic description of the polymer melt. We use the iterative Boltzmann inversion (IBI) procedure and a pressure-correction function to map the thermodynamic conditions of the atomistic configurations. The coarse-grained models are incorporated in the dissipative particle dynamics (DPD) method. The thermodynamic, structural, and dynamical properties of the *cis*-1,4-polybutadiene melt are very well reproduced by the coarse-grained DPD models with a significative computational gain. We complete this study by addressing the challenging question of the investigation of the shear modulus evolution. As expected from experiments, the stress correlation functions show behaviors that are dependent on the molecular weights defining unentangled and weakly entangled polymer melts.

1. INTRODUCTION

The relationship between the complex viscoelastic properties of polymers and their microscopic structures is a key issue in modern polymer materials science. A deep investigation of this structure−property relationship would allow designing materials tailored for particular applications, but it remains a major challenge. Atomistic simulations could be a possibility to identify the relationships between the chemical structure and the mechanical properties, but they remain problematic for polymeric systems due to the large time and length scales needed to track the evolution of these systems for times comparable to their longest relaxation times. Actually, the atomistic simulations of macromolecular systems demand modeling on a hierarchy of length and time scales spanning several orders of magnitude. For example, in a melt of a moderate molecular weight, the size of the atomistic constituents is on the order of 1 Å and the fastest motions are at times on the order of 10^{-14} s whereas collective relaxation in the system can occur on a scale of micrometers and a time that exceeds 1 ms.

One solution to simulating these time and length scales consists of reducing the degrees of freedom by coarsening the model. Each interaction center (called "bead") may represent then a few atoms or several monomers considering that not all atomistic details are essential for predicting many physical properties of polymers. There is no unique way to construct coarse-grained (CG) models of polymers.[1−14] The choice of the model depends on the physical properties that we want to predict. The off-lattice[15−19] and lattice models[20] have been widely applied to reproduce some physical properties of generic polymers. Other generic coarse-grained models have been used in order to simulate dynamical and rheological properties of long chains.[6,7,21,22] These models have been incorporated in Newtonian, simple Langevin, or Brownian dynamics methods.

Numerous coarse-graining approaches[3,4,9,11,14,23−32] have been developed in the past to conserve chemical information at the mesoscopic length scales. The idea behind the CG approach is to map atomistic configurations onto a coarser configuration in order to make simulations over longer time and length scales. The multiscale coarse-graining approach introduced by Izvekov and Voth[33,34] uses a variational procedure to build effective coarse-grained interactions from atomistic configurations. The reader is directed to the papers of Noid[29] and Akkermans[3,4] as well as the original works of Izvekov and Voth[33,34] for an overview of this CG technique. Another strategy[32] takes the route of constructing mesoscopic models from atomistic simulations of constrained clusters with a constant radius of gyration. An third alternative is the iterative Boltzmann inversion (IBI)[27] procedure. This is an iterative method for potential inversion from distribution functions using the potential of mean force approach.[35] CG intramolecular and intermolecular potential functions can be then deduced from appropriate distribution functions of atomistic configurations.[11,27,28,31]

The iterative Boltzmann inversion (IBI) procedure has been successfully applied to a variety of polymer melts formed by vinyl polymer chains,[36] dendrimers,[37] polystyrene,[13,38,39] and polyethylene chains.[11,28,31] These coarse-grained models have been implemented in either molecular dynamics[12,36−39] or dissipative particle dynamics[11,13,28,31] methods. These works have shown that the CG models cannot reproduce all properties of polymer melts as well as the atomistic models. Key questions[12,39] were addressed concerning the transferability of the CG models for different thermodynamic conditions and various families of polymers. When the dissipative forces are present in the simulations, another issue concerns the choice of the friction coefficient[11,31,39] that has been shown to have a significant impact on the dynamical properties of the polymer chains.

Received: July 7, 2012
Published: September 13, 2012

The dissipative particle dynamics (DPD)[40] method is a promising simulation technique that might bridge the gap between atomistic and mesoscopic simulations. DPD is a stochastic dynamics method in which the individual particles (beads) represent a set of atomistic degrees of freedom. As a consequence of this coarse graining, the conservative interactions are soft.[41] The dissipative and Brownian forces are short-ranged and pairwise additive so that the hydrodynamics of the fluid can satisfy the Navier−Stokes equation in the case of flowing. There are two major advantages to the DPD method. First, the soft potential allows for a time step that is up to 2 orders of magnitude larger than those typically used in molecular dynamics (MD) simulations. Second, the method, unlike the Brownian dynamics technique, includes a better description of hydrodynamic interactions. The original version of the DPD methodology has received substantial theoretical support concerning the extension of the DPD for the conservation of the total energy,[42−44] the incorporation of the electrostatic interactions,[45−48] and the modeling of entanglements by avoiding bond crossings.[49,50] The multibody DPD method (MDPD) has also been established[51−54] to model liquid−vapor interfaces. DPD simulations have been carried out to study polymer melts,[55,56] surfactant solutions,[57] and polymers at interfaces.[47,58−60] However, in these earlier DPD simulations of polymers, the parameters were not related to molecules of a specific chemistry and were chosen to match some macroscopic properties.[6,11,40,61] Nevertheless, some works[31,62−64] have tried to apply the DPD model using a molecular-specific parametrization.

In this work, our objective is to develop a CG model for *cis*-1,4-polybutadiene (*cis*-1,4-PB) (see Figure 1) for the DPD method in order to qualitatively predict the plateau modulus. The CG model of *cis*-1,4-PB is refined using the IBI technique. The transferability of the CG model is tested on the density and end-to-end distance obtained from both atomistic models and experiments.[65] We took the route of using this polymer because polybutadienes play a major role in rubber technology and the combination of its simple structure with the wealth of experimental and theoretical (force field parameters) data makes it ideal for validating our multiscale approach.

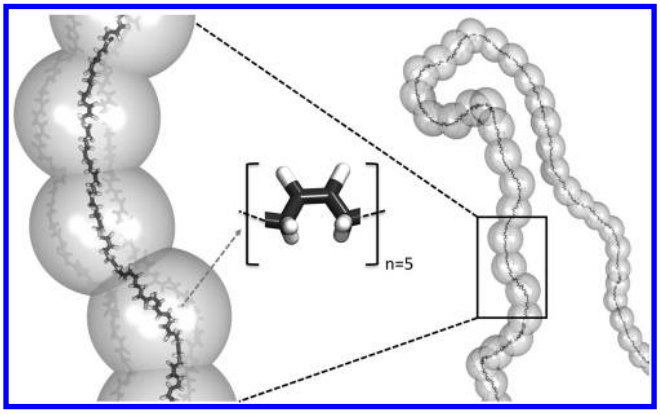

Figure 1. Coarse-grained description of *cis*-1,4-polybutadiene. A polymer bead represents five monomers of chemical structure C_4H_6.

The key questions pertinent to the multiscale strategy reported here that we want to address are the following: Is it possible to develop a DPD mesoscopic model from atomistic simulations to reproduce qualitatively the viscoelastic properties of *cis*-1,4-PB? How sensitive are the CG interactions to predict both thermodynamic and structural properties? How is the coarse-grained description temperature dependent? How much computational time is saved upon using the DPD method?

In section 2, we present the standard atomistic model, the IBI technique, and the DPD method. In section 3, we compare the results of the CG model with those resulting from the atomistic model and experiments. Finally, we conclude in section 4 by providing a brief summary of our main results and addressing the key points for the next mesoscopic simulations.

2. MODELS AND SIMULATION METHODS

2.1. Atomistic Simulations. The molecular dynamics (MD) simulations of bulk *cis*-1,4-polybutadiene were performed using the united atom force field developed by Smith and Paul.[66] The bulk configurations consisted of 40 chains with 400 and mainly 800 united carbons per chain. Chains formed by 800 united carbon atoms correspond to chains of 200 monomers and 10 800 g mol^{-1}. The constant-NpT simulations were performed using the Nosé−Hoover algorithm[67] at different temperatures under 0.1 MPa using 0.2 and 0.5 ps for the thermostat and barostat relaxation times, respectively. The equilibration of the polymer melt at a given temperature T was performed by successive simulations at 800 K and T. The equations of motion were integrated using the Verlet leapfrog algorithm scheme with a time step of 2 fs. The cutoff radius for the Lennard-Jones interactions was fixed at 14 Å. A typical MD simulation consists of an equilibration period of 10 ns and an additional production phase of 50 ns.

2.2. Dissipative Particle Dynamics (DPD). The dissipative particle dynamics method solves the Newtonian equations for particles subject to conservative, dissipative, and random forces. Thus

$$\frac{\mathrm{d}\mathbf{r}_i}{\mathrm{d}t} = \mathbf{v}_i, \qquad m_i \frac{\mathrm{d}\mathbf{v}_i}{\mathrm{d}t} = \mathbf{f}_i \tag{1}$$

where $\mathbf{f}_i$ is a pairwise-additive force defined as the sum of three contributions:

$$\mathbf{f}_i = \sum_{j \neq i} (\mathbf{f}_{ij}^{\mathrm{C}} + \mathbf{f}_{ij}^{\mathrm{R}} + \mathbf{f}_{ij}^{\mathrm{D}}) \tag{2}$$

where $\mathbf{f}_{ij}^{\mathrm{C}}$, $\mathbf{f}_{ij}^{\mathrm{R}}$, and $\mathbf{f}_{ij}^{\mathrm{D}}$ are the conservative, random, and dissipative forces, respectively. The conservative repulsive force $\mathbf{f}_{ij}^{\mathrm{C}}$ derives from a soft interaction potential and is expressed as

$$\mathbf{f}_{ij}^{\mathrm{C}} = \begin{cases} -\dfrac{\mathrm{d}w_{\mathrm{c}}(r_{ij})}{\mathrm{d}r_{ij}}\,\hat{\mathbf{r}}_{ij} & (r_{ij} < r_{\mathrm{c}}) \\ 0 & (r_{ij} \geq r_{\mathrm{c}}) \end{cases} \tag{3}$$

where $w_{\mathrm{c}}(r_{ij})$ is the conservative potential, r_{ij} is the relative displacement of particles i and j, and $\hat{\mathbf{r}}_{ij}$ is the corresponding unit vector. r_{c} is the cutoff radius and fixed at 4.0 nm. The dissipative and random forces are given by

$$\mathbf{f}_{ij}^{\mathrm{D}} = -\gamma\omega^{\mathrm{D}}(r_{ij})(\hat{\mathbf{r}}_{ij}\cdot\mathbf{v}_{ij})\hat{\mathbf{r}}_{ij} \tag{4}$$

$$\mathbf{f}_{ij}^{\mathrm{R}} = \sigma\omega^{\mathrm{R}}(r_{ij})\theta_{ij}\frac{1}{\sqrt{\delta t}}\hat{\mathbf{r}}_{ij} \tag{5}$$

where δt is the time step. $\mathbf{v}_{ij} = \mathbf{v}_i - \mathbf{v}_j$ is the relative velocity; the terms $\omega^{\mathrm{D}}(r_{ij})$ and $\omega^{\mathrm{R}}(r_{ij})$ are dimensionless weighting functions. σ is the amplitude of the noise; θ_{ij} is a random

dx.doi.org/10.1021/ct300582y | J. Chem. Theory Comput. 2012, 8, 4570−4579

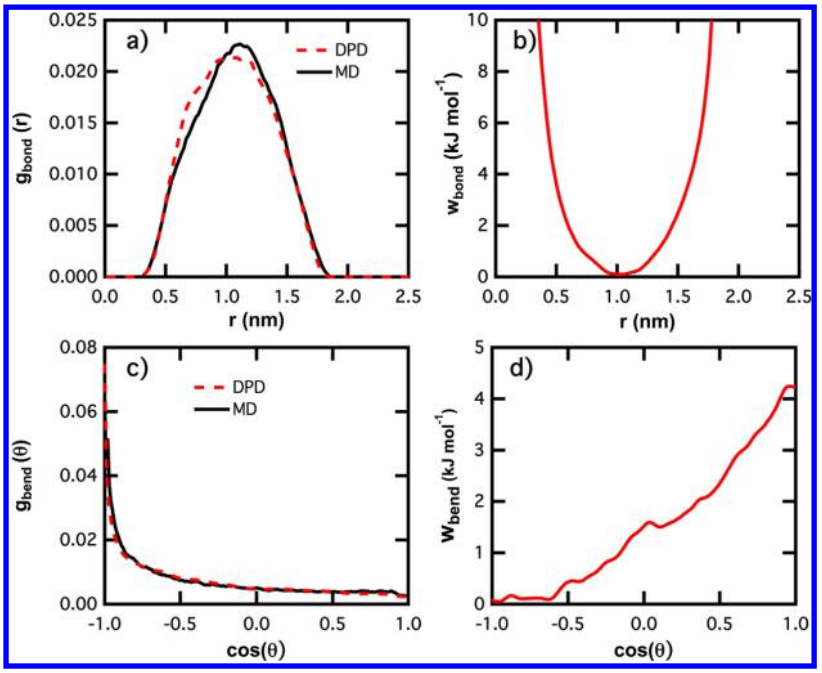

Figure 2. (a) Bonding and (c) bending CG distribution functions built from atomistic MD simulations for *cis*-1,4-PB. Corresponding (b) bonding and (d) bending CG potential functions obtained for a degree of coarse-graining of five monomers.

Gaussian number with zero mean and unit variance. γ and σ are the dissipation strength and noise strength, respectively. Espanol and Warren[68] have shown that the system will sample the canonical ensemble and obey the fluctuation−dissipation theorem if the following conditions are satisfied.

$$\gamma = \frac{\sigma^2}{2k_BT} \qquad \text{and} \qquad \omega^D(r_{ij}) = (\omega^R(r_{ij}))^2 \tag{6}$$

where k_B is Boltzmann's constant, T is the temperature, and $\omega^D(r_{ij}) = (1 - r/r_c)^2$.

The conservative potential $w_c(r_{ij})$ sums intramolecular and intermolecular interactions that will be calculated using the procedure in section 2.3.

2.3. Coarse-Graining Procedure. The degree of coarse-graining was fixed at 5, indicating that each bead corresponds to five monomers or 20 united atoms. The mass of the polymer bead is approximately 9 times smaller than the entanglement mass.[65] This level of coarse-graining allows a reproduction of the structure of the entangled polymer chains and the use of a larger time step. With this degree of 5, no bond crossings are detected in the simulation of the polymer chains leading to no topology violations on the polymer dynamics.[6] The polymer chain is then formed by 40 beads. From 10 independent atomistic configurations, we built bead−bead intermolecular and intramolecular potential functions calculated by coarse-graining atomistic configurations. Three different distribution functions are developed: the radial distribution function $g_{bond}(r_{i,i+1})$ between two consecutive beads in the polymer chain; the radial distribution function $g_{bend}(\theta_{i,i+1,i+2})$ between three consecutive beads in the polymer chain; the radial distribution function $g_{nb}(r_{i,j})$ between beads i and j of different polymer chains and beads i and j of the same molecule separated by more than one bond. From these radial distribution (RDF) functions, we use the potential of mean force approach[35] to derive the corresponding coarse-grained potential functions as

$$w^0_{bond}(r_{i,i+1}) = -k_BT \ln g_{bond}(r_{i,i+1}) \tag{7}$$

$$w^0_{bend}(\theta_{i,i+1,i+2}) = -k_BT \ln g_{bend}(\theta_{i,i+1,i+2}) \tag{8}$$

$$w^0_{nb}(r_{i,j}) = -k_BT \ln g_{nb}(r_{i,j}) \tag{9}$$

where $w^0_{bond}(r_{i,i+1})$, $w^0_{bend}(\theta_{i,i+1,i+2})$, and $w^0_{nb}(r_{i,j})$ are the coarse-grained potentials corresponding to the bonding, bending, and nonbonded interactions developed from the CG atomistic configurations. To improve the statistics, we have adopted the strategy[28] consisting of using different ways of grouping the five monomers in the atomistic configurations. The resulting potential functions have been tabulated: the forces are then obtained by a cubic spline interpolation.[69]

A first DPD simulation of 10 000 steps was performed with the initial $w^0_{bond}(r_{i,i+1})$, $w^0_{bend}(\theta_{i,i+1,i+2})$, and $w^0_{nb}(r_{i,j})$ potentials with 40 polymer chains of 40 beads using a time step of 50 fs. From these mesoscopic simulations, we recalculate the corresponding radial distribution functions $g^n_{bond}(r_{i,i+1})$, $g^n_{bend}(\theta_{i,i+1,i+2})$, and $g^n_{nb}(r_{i,j})$, respectively. We observe that the target RDFs in eqs 7−9 are not accurately reproduced. By calculating the ratio between these intermediary RDFs and the target RDFs according to the iterative Boltzmann inversion process, we obtain new potential functions as

$$w^{n+1}(r) = w^n(r) + k_BT \ln\left(\frac{g^n(r)}{g(r)}\right) \tag{10}$$

where $g^n(r)$ and $w^n(r)$ refer to the bonding, bending, and nonbonded distribution and potential functions at step n, respectively. $g(r)$ is the target RDF. This scheme is reiterated until convergence is obtained.

An iteration consists of a constant-NVT DPD simulation of 10 000 steps, and five iterations were required to obtain a good convergence. Parts a and c of Figure 2 show that the intramolecular target RDFs obtained from atomistic simulations are very well reproduced by the CG models after the

iterative process. The resulting CG potential functions, used in the DPD simulations, are given in parts b and d of Figure 2 for the bonding and bending energy contributions, respectively. It is worth noting that the coarse-grained potential for the bond stretching resembles a simple harmonic potential that has been widely applied to model the interactions between consecutive beads.[27,50,58,70] In the same spirit, angular potentials seem to disfavor the small angle values in line with what has been done for generic coarse-grained models by the use of artificial angular potentials to make the chains more or less flexible.[71]

Figure 3a shows the radial distribution function between nonbonded beads calculated from atomistic configurations and

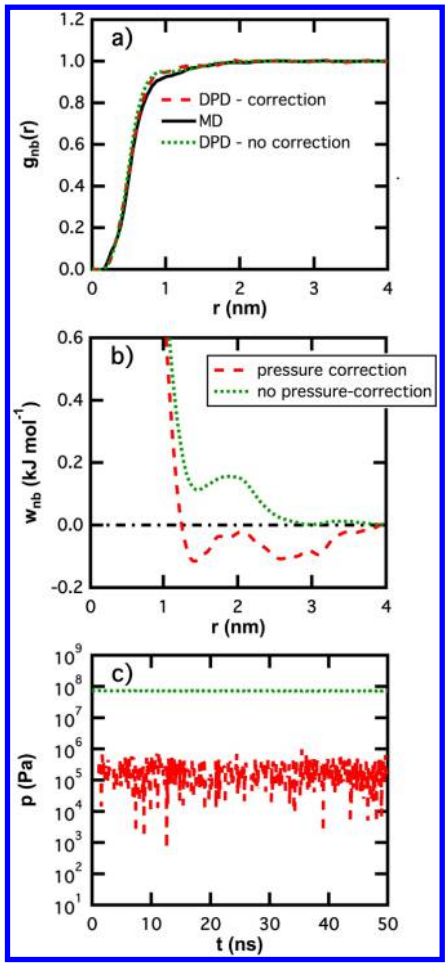

Figure 3. (a) Nonbonded pair radial distribution functions calculated from MD simulations. (b) Potential of mean forces used in DPD simulations calculated with and without the pressure correction. (c) Calculated pressures in the DPD simulations with and without the pressure correction.

DPD simulations. We also observe a good agreement between these distribution functions. The corresponding CG potential is given in Figure 3b. However, this potential gives an average pressure of 72 MPa that deviates significantly with the thermodynamic conditions (T = 298 K, p = 0.1 MPa) of the atomistic configurations. This shows the inability of the constant-NVT CG model to accurately describe a bulk submitted to experimental conditions. As already underlined by Reith,[27] we modify the coarse-grained potential by an attractive linear tail function defined by $A(1 - r/r_c)$. The corrected CG potential is then used to perform new constant-NpT DPD simulations in order to calculate the pressure and the nonbonded RDF. After five iterations within the IBI procedure, the resulting CG potential, shown in Figure 3b, leads to the convergence of the pressure at 0.1 MPa. Figure 3c shows the evolution of the pressure as a function of time for the two nonbonded CG potentials. These curves allow checking that the corrected-CG potential reproduces accurately the target pressure with a pressure trajectory in line with a system at mechanical equilibrium. Whereas this potential was purely repulsive when no pressure correction was applied, it becomes attractive with the correction. Nevertheless, this pressure correction does not have an impact on the shape of the RDF between nonbonded polymer beads (see Figure 3a) and the agreement with the target RDF remains excellent. In addition, the repulsive part of the two nonbonded CG potentials at short separation distances is also consistent with the use of the Lennard-Jones 12−6 potential form in a large number of simulations of CG polymer chains.[22,72−75] We also check the topology violations by using the method developed in ref 49. With the use of the CG potentials developed here, we detect no bond crossings in the simulation of the polymer melt at a mesoscopic level. This means that no additional spring−spring potential is required with our CG potentials to prevent unphysical bond crossings,[6−8] contrary to what was observed in DPD simulations with standard soft potentials.[49,50]

3. RESULTS AND DISCUSSION

Figure 4a shows the specific volume versus temperature diagram for *cis*-1,4-PB. The molar volume is calculated from constant-NpT MD simulations in the 50−300 K temperature range. The temperature dependence of the simulated specific volume establishes a change in the slope of the linear variation of the volume with the temperature for a temperature which is

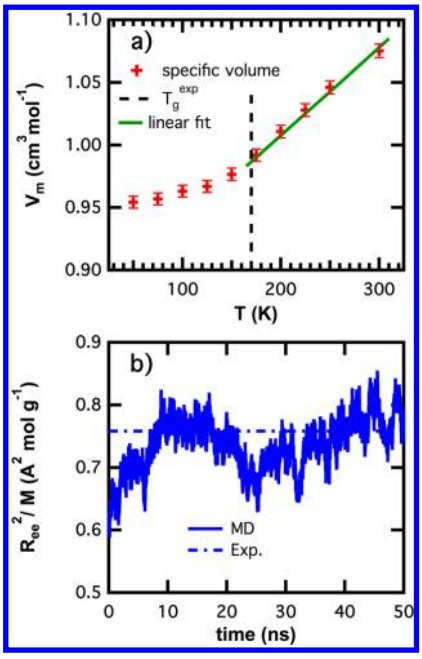

Figure 4. (a) Molar volume as a function of the temperature calculated from atomistic MD simulations. The vertical line indicates the experimental glass transition temperature, and the solid line represents the linear fit over the temperature dependence of the volume above the glass transition temperature. (b) Trajectory of the mean square end-to-end distance obtained from MD simulations.

dx.doi.org/10.1021/ct300582y | J. Chem. Theory Comput. 2012, 8, 4570−4579

slightly smaller than the experimental glass transition temperature. The force field used allows a qualitative prediction of the glass transition temperature. Above the glass transition temperature, the linear temperature dependence of the molar volume on the temperature yields a thermal expansion coefficient $\alpha_p = (1/V)(\partial V/\partial T)_p$ of 6.5×10^{-4} K^{-1} that agrees very well with the experimental value[76] of 6.7×10^{-4} K^{-1}. This establishes that our atomistic simulations are well adapted to temperatures above the glass transition temperature.

The simulated density is 0.93 ± 0.01 g cm^{-3} at 298 K, whereas previous works[66,77] found 0.91 g cm^{-3} with the same force field. This deviation of 2% is explained by the dependence of the density on the chain length that shows an increase of the melt density with the chain length.[77] Our atomistic simulations used 40 chains of 200 monomers, whereas the other molecular simulations have been performed with 40 chains of 25 monomers. This deviation of 2% is exactly that which is expected from the chain length dependence.[77] For completeness, we have checked that modeling a chain length of 25 monomers leads to a polymer melt density of 0.91 g cm^{-3}. Figure 4b shows the trajectory of the mean square end-to-end distance over 50 ns. This property was time-averaged over all the chains in the melt. The ratio of the mean square end-to-end distance to the molecular weight of the polymer chain is 0.74 ± 0.03 Å^2 mol g^{-1}, whereas the experimental ratio is 0.76.[65] This also confirms a good reproduction of the structural properties of *cis*-1,4-PB in the bulk amorphous phase.

The dynamical properties of the bulk *cis*-1,4-PB are illustrated in Figure 5 through the end-to-end vector

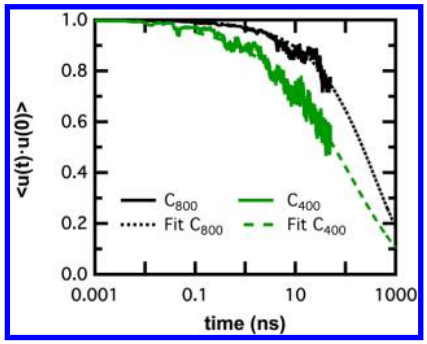

Figure 5. End-to-end vector orientational autocorrelation function calculated using atomistic MD simulations for two different polymer chain lengths C_{400} and C_{800}. The dotted lines represent the fits obtained using $\exp(-t/\tau_k)^{\beta_k}$.

autocorrelation function calculated with two different polymer chain lengths. This function measures the rate of the overall chain relaxation or how fast the chain forgets its initial configuration. Interestingly, the function $\langle \mathbf{u}(t)\cdot\mathbf{u}(0)\rangle$, where $\mathbf{u}$ is the unit vector directed along the chain end-to-end vector, does not decay to zero by the end of the 50 ns. As observed in Figure 5, the decorrelation of the polymer melt slows down as the chain length increases. We check in Figure 5 that these autocorrelation functions are well described by a stretched exponential $\exp[-(t/\tau)^{\beta}]$, where τ is the Rouse relaxation time and $\beta < 1$, suggesting the presence of entanglement effects. The values of τ and β are given in Table 1. Actually, we observe the decrease of β with increasing molecular weight. The fitted decorrelation curve would show that the end-to-end vector autocorrelation approaches zero at times of a microsecond, i.e., $\tau \approx 1$ μs. A complete relaxation would imply a simulation of 1

Table 1. Relaxation Time τ and β Parameters Calculated from the Fitting of the End-to-End Vector Autocorrelation Function Using $\exp[-(t/\tau)^{\beta}]$[a]

chain length	τ (ns)	β	D (10^{-7} cm^2 s^{-1})
C_{80}	1.3	0.91	13.5
C_{160}	11	0.80	5.2
C_{800}	221	0.65	1.0

[a] D is the diffusion coefficient of the coarse-grained models for different chain lengths calculated from the mean square center-of-mass displacement.

year over 12 processors with the system size studied here. It highlights the limits of the atomic description for the investigation of properties of entangled polymers for large time scales.

Mesoscopic simulations of *cis*-1,4-PB were performed with 40 chains of 40 beads at 298 K at a constant pressure of 0.1 MPa using the Berendsen algorithm.[78] The time step was fixed at 50 fs. The cutoff radius r_c was set to 4 nm, and the friction coefficient γ was kept at 300 kg mol^{-1} ns^{-1}. It is well-known that the dynamical properties of polymer melts can be significantly affected by the choice of the adjustable parameters[11,13] r_c and γ. On the basis of the work[11] of Lahmar and Rousseau, who have studied the influence of r_c and γ on the global and local dynamics of a polymer melt, we checked that γ = 300 kg mol^{-1} ns^{-1} was a good choice for the observation of long-time dynamical processes. It is also possible to rescale γ to reproduce accurately the dynamical experimental data.[10,11,13] The temperature was fixed at 298 K, leading to k_BT = 2.48 kJ mol^{-1}. The unit of mass is the mass of one bead that corresponds to five monomers of PB (m_i = 270 g mol^{-1}). The conservative potential used in DPD simulations $w_c(r_{ij})$ sums $w_{bond}(r_{i,i+1})$, $w_{bend}(\theta_{i,i+1,i+2})$, and $w_{nb}(r_{i,j})$ represented in Figures 2b, 2c, and 3b, respectively. The calculation of the density of the polymer melt was carried out by constant-NpT DPD simulations with an acquisition phase of 4×10^6 steps corresponding to a real time of 200 ns. We used a barostat mass Q_p = 0.1 MPa s. Figure 6a shows the evolution of the density of the *cis*-1,4-PB melt at 298 K as a function of time calculated from DPD simulations in the NpT statistical ensemble. We also report the evolution resulting from the atomistic simulation over a shorter period. The average of the melt density is 0.96 ± 0.02 g cm^{-3} against 0.93 for MD, leading to deviations of 3% from atomistic models. This means that the pressure correction incorporated in the optimization of the CG potentials allows reproducing very well the atomistic simulations. The agreement with experiments is a little less good with a deviation of 5%. However, we believe that a better reproduction of the experimental data can still be achieved by using an atomistic potential that better reproduces the experimental density. Anyway, this represents a promising step toward the prediction of thermodynamic properties of macromolecular systems with a coarse-grained description. The question of temperature transferability remains a challenging task and an open question. At this point, Figure 6b shows the temperature dependence of the density calculated from DPD simulations over the 250−350 K temperature range. An estimate of the thermal expansion coefficient α_p gives 6.2×10^{-4} K^{-1}. This corresponds to a deviation of 8% from experiments and shows a qualitative prediction of the density at this temperature range. However, the calculation of the isothermal compressibility κ_T from volume fluctuations of the CG model in the NpT ensemble

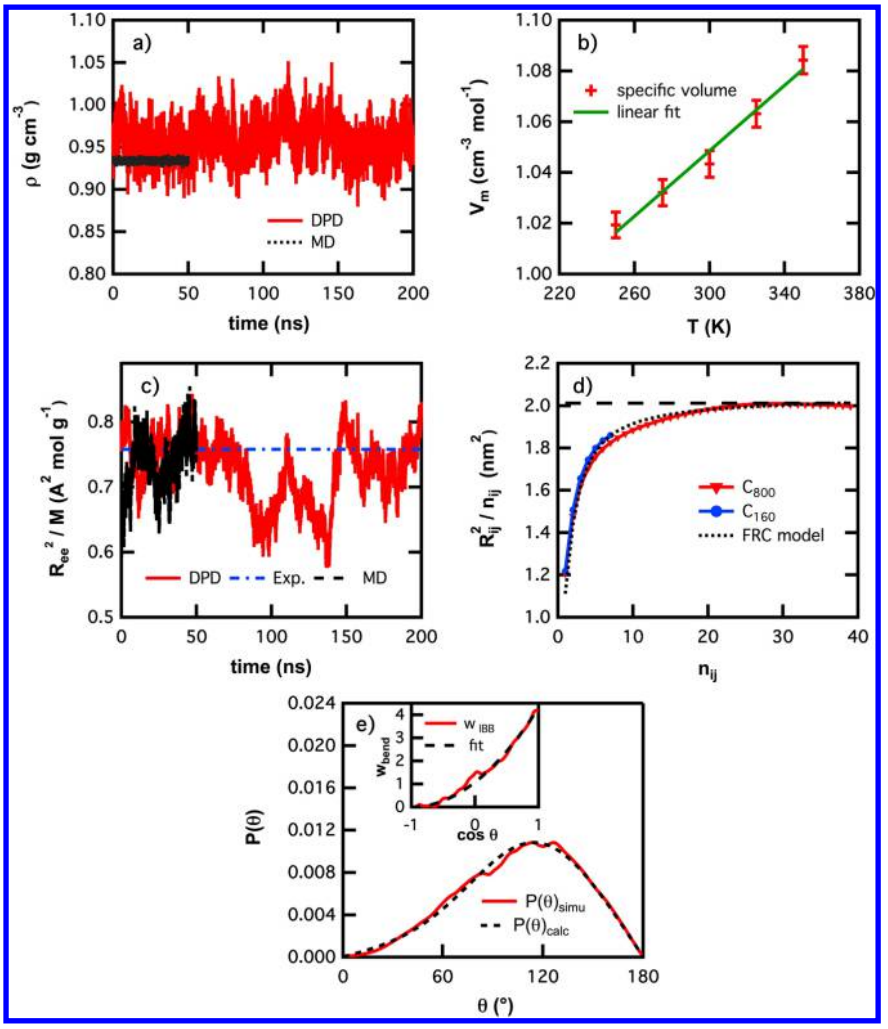

Figure 6. Thermodynamic, structural, and dynamical properties of the coarse-grained models. (a) Density of the *cis*-1,4-PB melt calculated using DPD simulations as a function of time. (b) Temperature dependence of the density calculated using the CG description. The solid line shows the linear fit providing the value of the thermal expansion coefficient. (c) Mean square end-to-end distance as a function time along with the value given by atomistic models. (d) R_{ij}^2/n_{ij} ratio as a function of the number of beads for two molecular weights. The ratio predicted by the freely rotating chain (FRC) model is represented by dotted lines. (e) Simulated and calculated angular probabilities $P_{bend}(\theta)$. The inset shows the fit of the angular potential using a quadratic function.

gives a value close to 1.0×10^{-11} Pa^{-1} according to $\kappa_T = -[(\langle V^2\rangle - \langle V\rangle^2)/k_BT\langle V\rangle]$ for the C_{800} chain length. The deviation of 1 order of magnitude from experiments[76] shows the pressure dependence of the CG potentials[38] developed from the IBI method. Even if the CG potentials are necessarily dependent on thermodynamic conditions which were used for their development, the CG model is found here to be temperature transferable in a relatively large temperature range indicating a weak temperature dependence of the different RDFs.

We now focus on the structural and dynamical properties of the coarse-grained models. Figure 6c shows the mean square end-to-end distance averaged over all the chains as a function of time calculated using DPD and MD simulations in the NpT ensemble. The average end-to-end distance calculated by the coarse-grained description is 0.74 ± 0.05 Å^2 mol g^{-1} and matches the experimental value very well with a deviation of only 3%. The ratio of the mean square end-to-end distance to the squared radius of gyration is 6.1 ± 0.2, whereas a ratio of 6 is expected for ideal chains in a polymer melt.

We plot in Figure 6d the quantity R_{ij}^2/n_{ij} as a function of the number of bonds in a subchain. R_{i-j} is the mean distance of the subchain formed by n_{ij} bonds. This quantity increases monotonically with the number of beads until it reaches a plateau. The asymptotic value of 2.0 nm^2 is calculated from the quantity $M_oR_{ee}^2/M$, where M_o is the molar mass of the bead and R_{ee}^2/M = 0.74 Å^2 mol g^{-1}. This limit value is represented in Figure 6c by a dotted line. For the C_{160} chain length, we check that this chain length is not large enough to reach the limiting value. Nevertheless, we observe the same n_{ij} effects on the subchain distance as those of equilibrated long chains for the first 10 beads. For the C_{800} chain length, the quantity converges slowly toward its theoretical limiting value in line with well-equilibrated long chains. We also plot the behavior of the R_{ij}^2/n_{ij} expected from the freely rotating chain model[79] using chains with n_{ij} bonds, each of length l_{ij} = 1.05 nm and bond angle cos θ_{ijk} = −0.296 averaged over all the bond angles of the chains. This ratio is then represented within the free rotating chain model by

dx.doi.org/10.1021/ct300582y | J. Chem. Theory Comput. 2012, 8, 4570−4579

$$\frac{\langle R_{i-j}{}^2\rangle}{n_{ij}} = \left[\frac{1-\cos\theta_{ijk}}{1+\cos\theta_{ijk}} + \frac{2\cos\theta_{ijk}[1-(-\cos\theta_{ijk})^{n_{ij}}]}{(1+\cos\theta_{ijk})^2}\frac{1}{n_{ij}}\right] l_{ij}{}^2 = C_{n_{ij}} l_{ij}{}^2 \quad (11)$$

where $C_{n_{ij}}$ is Flory's characteristic ratio.[80] For large numbers of bonds ($n_{ij} \to \infty$), the characteristic ratio saturates at a finite value $C_\infty \approx R_{ee}{}^2/(nl^2)$ (plateau shown in Figure 6d), where n and l are the number of bonds in the polymer chain and the bond length, respectively. The comparison with this model is pertinent because no torsional potentials are used in our CG model. As checked in Figure 6d, the simulated ratio of the CG model is in perfect agreement with that predicted by the freely rotating chain model (FRC) from the short subchain lengths to the long-chain linear region. This is a clear indication that the equilibration of the CG chains has been achieved at all length scales. Since the polymer configuration is accurately described by the FRC model, we can expect that the angular distribution is governed by the angular potential. The simulated angular distribution for the CG model is shown in Figure 6e along with the probability $P_{bend}(\theta)$ of the bond angle θ obtained from $w_{bend}(\theta)$ alone.

$$P_{bend}(\theta) = A \sin\theta \exp\left(-\frac{w_{bend}(\theta)}{k_B T}\right) \quad (12)$$

$P_{bend}(\theta)$, shown in Figure 6e, is calculated by fitting the $w_{bend}(\theta)$ potential of Figure 2d with a quadratic $C[\cos(\theta)+1]^2$ equation shown in the inset of Figure 6e. In eq 12

$$A = \frac{2\pi\sqrt{C/k_B T}}{180\sqrt{\pi}\ \mathrm{erf}(2\sqrt{C/k_B T})}$$

is calculated from $\int_0^\pi P_{bend}(\theta)\, d\theta = 1$. We observe then that the simulated angular distribution averaged over all the chains and bond angles agrees very well with the probability $P_{bend}(\theta)$, indicating that the behavior of the simulated P_{bend} is mainly governed by the bond angle potential.

The long-time dynamics of the simulated *cis*-1,4-PB melt has been investigated by calculating the end-to-end vector autocorrelation function shown in Figure 7a for three chain lengths. We check that the function of the C_{80} chain length approaches the zero value in a few nanoseconds whereas the decorrelation curve of the longest C_{800} chain length reaches zero at a few hundreds of nanoseconds in agreement with the Rouse relaxation time and fitted decorrelation curve obtained from our atomistic simulations. This also shows that the DPD simulations with the use of CG models is able to reach these time scales characteristic of the relaxation of polymer melts with a reduced computational effort. Actually, the simulation of a polymer melt over 1 μs requires 5 days for DPD simulations and 500 days for atomistic simulations over 12 processors at a time. This makes these coarse-grained models very attractive for the prediction of thermodynamic, structural, and dynamical properties of polymer systems.

The mean square displacement (MSD) of the polymer beads is given in Figure 7b as a function of time for three polymer melt systems. As expected from the degree of coarse-graining, the ballistic regime (scaling as t^2) cannot be observed due to the length scale imposed by the size of the bead. However, it impacts the Rouse regime by increasing the slope of the MSD

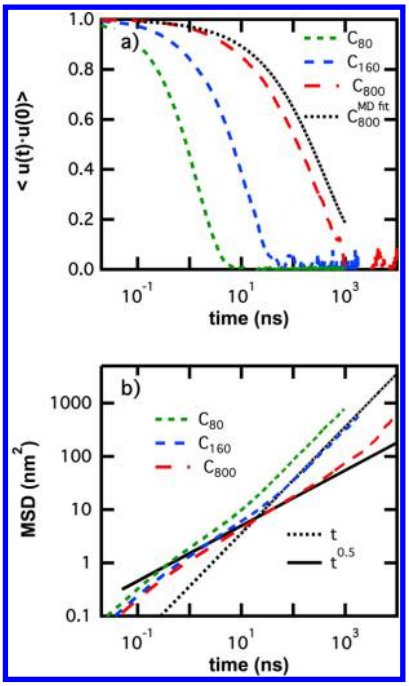

Figure 7. (a) End-to-end vector orientational autocorrelation function calculated using coarse-grained models for the C_{80}, C_{160}, and C_{800} polymer chain lengths. The fit calculated from atomistic simulations over C_{800} chains is shown for comparison. (b) Mean square displacement of the polymer beads for the C_{80}, C_{160}, and C_{800} polymer melt systems. The Einstein regime (slope equal to 1) and Rouse regime (slope equal to 0.5) are marked by dotted and dashed lines, respectively.

that becomes slightly larger than 0.5.[81] For the shortest chain length studied here, we observe a transition from the Rouse regime (scaling as $t^{0.5}$) to the Einstein regime (scaling as t) at the relaxation time of a few nanoseconds. It is again observed for the C_{160} polymer length but at a larger time, as expected from the Rouse time of this chain. For the longest polymer chain, the crossover from the Rouse to Einstein diffusion occurs at a few hundreds of nanoseconds. We also observe a slowdown in the Rouse regime compared to the shortest chains, but the chains are not enough entangled to observe a slope of 0.25 (reptation model[21,82]) in line with the observation of the $G(t)$ curve discussed in what follows. The dynamical properties of the CG model follow the behaviors expected by the Rouse theory. Additionally, Table 1 show that β is close to 1 for a short polymer chain length and that it deviates further from 1 with increasing polymer chain lengths. From the long-time limit of the curves for C_{160} and C_{80} in Figure 7b, we obtain a diffusion coefficient on the order of 10^{-7} cm^2 s^{-1} that agrees very well with those calculated with atomistic models.[14] This justifies the choice of γ of the dissipative force. We plan now to use the CG models to calculate the time-dependent shear stress relaxation modulus.

Before investigating the viscoelastic property of the *cis*-1,4-PB chains, we investigate the number of entanglements from the primitive path analysis (PPA).[83] Figure 8 shows a typical configuration of *cis*-1,4-PB chains of C_{800}. This configuration results from DPD simulations at 0 K by using the primitive path analysis (PPA): (i) the two ends of the polymer chains are fixed in space; (ii) the intramolecular interactions (bending, nonbonded) are set to zero; (iii) the intermolecular interactions are conserved and calculated with the $w_{nb}(r_{i,j})$

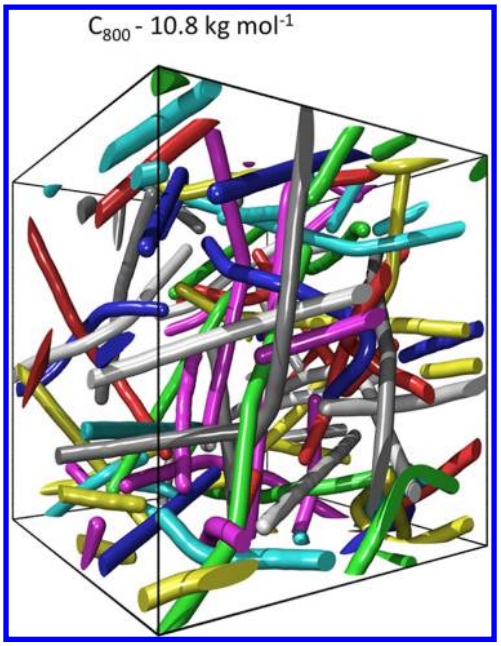

Figure 8. Configuration of the *cis*-1,4-PB melt obtained from DPD simulations using the primitive path analysis at 0 K.

potential; (iv) the bonding potential between two consecutive beads is replaced by the FENE potential defined as $-(kr_o^2/2)\log(1 - r^2/r_o^2)$, where k and r_o were set to 250.0 kJ mol^{-1} nm ^{2} and 4.0 nm, respectively. This PPA algorithm allows the quantitative determination of the number of entanglements per chain. The primitive path length, L_{pp}, is defined as $d_T M/M_e$, where d_T is the reptation tube diameter and M and M_e are the weight of the polymer chain and the molecular weight between entanglements, respectively. Since the reptation tube diameter d_T is related to M_e by

$$d_T^{\,2} = \frac{R_{ee}^{\,2}}{M} M_e \tag{13}$$

we obtain the following equation that allows estimating M_e from the PPA method:

$$M_e = \frac{R_{ee}^{\,2}}{L_{pp}^{\,2}} M \tag{14}$$

The average entanglement mass is found to be 2749 g mol^{-1} for the C_{800} chain length, whereas the value deduced from the plateau modulus[65] $M_e = 4\rho RT/5G_N^0$ is 2363 g mol^{-1} and the experimental value[65] is 2347 g mol^{-1}. This entanglement mass corresponds to an entanglement length N_e of 10 beads for C_{800} that compares very well with the theoretical value of 9. For this reason, we calculate then the shear relaxation moduli for different polymer chain lengths of C_{80}, C_{160}, and C_{800} that correspond to chains formed by 4, 8, and 40 beads, smaller and greater than N_e, respectively.

The shear relaxation modulus can be calculated from the autocorrelation of the stress tensor elements[73] as

$$G(t) = \frac{V}{5k_BT}\langle \sigma_{xy}(t)\sigma_{xy}(0) + \sigma_{yz}(t)\sigma_{yz}(0) + \sigma_{zx}(t)\sigma_{zx}(0)\rangle + \frac{V}{30k_BT}\langle N_{xy}(t)N_{xy}(0) + N_{yz}(t)N_{yz}(0) + N_{zx}(t)N_{zx}(0)\rangle \tag{15}$$

with $N_{\alpha\beta} = \sigma_{\alpha\alpha} - \sigma_{\beta\beta}$, where α and β denote the x, y, and z components. The components of the stress tensor are defined by

$$\sigma_{\alpha\beta} = -\frac{1}{V}\left(\sum m_i \mathbf{v}_i^\alpha \mathbf{v}_i^\beta + \frac{1}{2}\sum_{i\neq j} \mathbf{r}_{ij}^\beta \mathbf{f}_{ij}^{C,\alpha}\right) \tag{16}$$

where $\mathbf{f}_{ij}^{C,\alpha}$ is the α component of the conservative force defined in eq 3 and $\mathbf{v}_i^\alpha$ is the α component of the velocity of bead i.

We have calculated the stress tensor autocorrelation function from long DPD simulations in the NVT ensemble over 1 μs. In order to improve the accuracy of the time correlation function, we have used the multiple-tau correlator[84] on the fly during the DPD simulations using the correlator parameters $m = 2$ and $p = 16$.[84] By using the expressions given in eqs 16 and 15, we have calculated $G(t)$ for three polymer chain lengths, C_{80}, C_{160}, and C_{800}. The stress relaxation functions are reported in Figure 9.

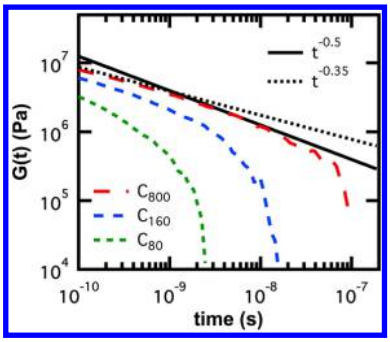

Figure 9. Stress relaxation function $G(t)$ calculated from DPD simulation over 1 μs time period for three polymer chain lengths. For completeness, dashed and dotted solid lines represent slopes of −0.5 and −0.35,[71] respectively.

As expected for unentangled chains, the $G(t)$ curves of the C_{80} and C_{160} polymer chains decay continuously. For the weakly entangled C_{800} polymer chain, we observe the same decay at short times as for C_{160}. This was already previously observed from simulations with generic models.[73] Additionally, the decay of the $G(t)$ for C_{800} is slowed at large times due to additional topological constraints for larger molecular weight but no plateau is observed. In fact, this is expected from experimental data where $N/N_e > 20$ is required to obtain a plateau. Interestingly, the scaling of the $G(t)$ curve with the mesoscopic model is in good agreement with the experimental data of polymers.[85] The slope before the deep decay ranges from −0.35 to −0.5. This is in line with both the Rouse models and the last results in ref 71, where the experimental data are numerically treated from sets of Maxwell modes (frequencies) to obtain a time-dependent shear modulus.

4. CONCLUSIONS

We have presented a multiscale approach in order to investigate the properties of polymer melts at long time scales. We have focused on the thermodynamic, structural, dynamical, and mechanical properties of *cis*-1,4-polybutadiene. The multiscale strategy, based upon a bottom-up approach, consists of building a coarse-grained model from an atomistic representation of the polymer melt. We have shown that the atomistic simulations reproduced the temperature dependence of the polymer melt density, the glass transition temperature, the thermal expansion coefficient, and the square end-to-end distance. As expected

from the atomistic description, we have checked that the MD simulations did not allow a complete relaxation of the polymer melt over the simulated time period.

Coarse-grained models have been developed using the iterative Boltzmann inversion (IBI) procedure and the potential of mean force approach. A coarse-grained model have been built to model bonding, bending, and nonbonded interactions. These potentials have been incorporated in a genuinely mesoscale method: the dissipative particle dynamics (DPD). We have also modified the coarse-grained potentials by a pressure-correction term in order to reproduce the thermodynamic conditions of the atomistic configurations. The advantage of this pressure correction in the coarse-grained models is the ability to accurately predict the polymer melt density. We have also established the inability of the constant-NVT CG model to accurately describe a bulk submitted to experimental conditions, particularly the temperature dependence of density, or for studies where stress plays a key role, e.g., the answer to a mechanical solicitation. As far as we know, these facts have never been pointed out. The end-to-end distance is also in good agreement with experiments, and the behavior of the CG chains is in line with that expected from the freely rotating chain model. We have also shown the temperature transferability of the coarse-grained model over a relatively large temperature range through a good estimate of the thermal expansion coefficient. The dynamics of the polymer chain has been analyzed through the decay of the end-to-end vector autocorrelation function that approaches zero at the microsecond time scale for the longest polymer chain length studied here, in line with expected behavior from atomistic simulations. From a computational viewpoint, modeling a polymer melt over 1 μs demands less than 1 week for DPD models and 70 weeks for an atomistic description. This clearly establishes the computational gain offered by the DPD simulations. The dynamics of the CG polymer chains has been investigated through the scaling of the mean square displacement. These MSD curves show transitions from Rouse to Einstein regimes at practically the Rouse time.

As stated in the Introduction, our long-term objective was the prediction of the viscoelastic properties of polymer melts. We have tried to calculate the stress relaxation function for three molecular weights. For the molecular weights investigated, the decay of the $G(t)$ curves follows the Rouse regime and no plateau region is observed. Only a slower decay is observed with the larger molecular mass. This is in line with recent studies that have shown that a polymer chain length above 20 N_e is required to observe the signature of the entanglement in the $G(t)$ curve.[86]

However, the multiscale approach developed here opens the way to quantitatively predict the viscoelastic properties of polymer melts: the challenge consists of predicting the plateau modulus as a function of the chemical nature of the polymer. This will be addressed in a future paper.

AUTHOR INFORMATION

Corresponding Author

*E-mail: Patrice.Malfreyt@univ-bpclermont.fr.

Notes

The authors declare no competing financial interest.

REFERENCES

(1) Murat, M.; Kremer, K. *J. Chem. Phys.* **1998**, *108*, 4340.
(2) Akkermans, R. L. C.; Briels, W. J. *J. Chem. Phys.* **2000**, *113*, 6409.
(3) Akkermans, R. L. C.; Briels, W. J. *J. Chem. Phys.* **2001**, *114*, 6210.
(4) Akkermans, R. L. C.; Briels, W. J. *J. Chem. Phys.* **2001**, *114*, 1020.
(5) Briels, W. J.; Akkermans, R. L. C. *Mol. Simul.* **2002**, *28*, 145.
(6) Padding, J. T.; Briels, W. *J. Chem. Phys.* **2001**, *115*, 2846.
(7) Padding, J. T.; Briels, W. J. *J. Chem. Phys.* **2002**, *117*, 925.
(8) Padding, J. T.; Briels, W. J. *J. Chem. Phys.* **2003**, *118*, 10276.
(9) Müller-Plathe, F. *ChemPhysChem* **2002**, *3*, 754.
(10) Kindt, P.; Briels, W. J. *J. Chem. Phys.* **2005**, *123*, 224903.
(11) Lahmar, F.; Rousseau, B. *Polymer* **2007**, *48*, 3584.
(12) Carbone, P.; Varzaneh, H.; Müller-Plathe, F. *J. Chem. Phys.* **2008**, *128*, 064904.
(13) Qian, H. J.; Liew, C. C.; Müller-Plathe, F. *Phys. Chem. Chem. Phys.* **2009**, *11*, 1962.
(14) Strauch, T.; Yelash, L.; Paul, W. *Phys. Chem. Chem. Phys.* **2009**, *11*, 1942.
(15) Grest, G. S.; Kremer, K. *Phys. Rev. A* **1986**, *33*, 3628.
(16) Baumgärter, A.; Binder, K. *J. Chem. Phys.* **1981**, *75*, 2994.
(17) Binder, K. *Computational Modelling of Polymers*; Marcel Dekker: New York, 1992.
(18) Grest, G. S. *Curr. Opin. Colloid Interface Sci.* **1997**, *2*, 271.
(19) Grest, G. S. *Adv. Polym. Sci.* **1999**, *138*, 149.
(20) Kremer, K.; Binder, K. *Comput. Rep.* **1988**, *7*, 259.
(21) Kremer, K.; Grest, G. S. *J. Chem. Phys.* **1990**, *92*, 5057.
(22) Kreer, T.; Muser, M. H.; Binder, K.; Klein, J. *Langmuir* **2001**, *17*, 7804.
(23) Tschöp, W.; Kremer, K.; Batoulis, J.; Bürger, T.; Hahn, O. *Acta Polym.* **1998**, *49*, 61.
(24) Meyer, H.; Biermann, O.; Faller, R.; Reith, D.; Müller-Plathe, F. *J. Chem. Phys.* **2000**, *113*, 6264.
(25) Reith, D.; Meyer, H.; Müller-Plathe, F. *Macromolecules* **2001**, *34*, 2335.
(26) Faller, R. *Polymer* **2003**, *45*, 3869.
(27) Reith, D.; Pütz, M.; Müller-Plathe, F. *J. Comput. Chem.* **2003**, *24*, 1624.
(28) Guerrault, X.; Rousseau, B.; Farago, J. *J. Chem. Phys.* **2004**, *121*, 6538.
(29) Noid, W. G.; Chu, J. W.; Ayton, G. S.; Krishna, V.; Izvekov, S.; Voth, G. A.; Das, A.; Andersen, H. C. *J. Chem. Phys.* **2008**, *128*, 244114.
(30) Noid, W. G.; Liu, P.; Wang, Y.; Chu, J. W.; Ayton, G. S.; Izvekov, S.; Andersen, H. C.; Voth, G. A. *J. Chem. Phys.* **2008**, *128*, 244115.
(31) Lahmar, F.; Tzoumanekas, C.; Theodorou, D. N.; Rousseau, B. *Macromolecules* **2009**, *42*, 7485.
(32) Lei, H.; Caswell, B.; Karniadakis, G. E. *Phys. Rev. E* **2010**, *81*, 026704.
(33) Izvekov, S.; Voth, G. A. *J. Phys. Chem. B* **2005**, *109*, 2469.
(34) Izvekov, S.; Voth, G. A. *J. Chem. Phys.* **2005**, *123*, 134105.
(35) Kirkwood, J. G. *J. Chem. Phys.* **1935**, *3*, 300.
(36) Milano, G.; Müller-Plathe, F. *J. Phys. Chem. B* **2005**, *109*, 18608.
(37) Carbone, P.; Negri, F.; Müller-Plathe, F. *Macromolecules* **2007**, *40*, 7044.
(38) Spyriouni, T.; Tzoumanekas, C.; Theodorou, D.; Müller-Plathe, F.; Milano, G. *Macromolecules* **2007**, *40*, 3876.
(39) Qian, H. J.; Carbone, P.; Chen, X.; Karimi-Varzaneh, H. A.; Liew, C. C.; Müller-Plathe, F. *Macromolecules* **2008**, *41*, 9919.
(40) Hoogerbrugge, P. J.; Koelman, J. M. V. A. *Europhys. Lett.* **1992**, *19*, 155.
(41) Klapp, S. H. L.; Diestler, D. J.; Schoen, M. *J. Phys.: Condens. Matter* **2004**, *16*, 7331.
(42) Avalos, J. B.; Mackie, A. D. *Europhys. Lett.* **1997**, *40*, 141.
(43) Espanol, P. *Europhys. Lett.* **1997**, *40*, 631.
(44) Avalos, J. B.; Mackie, A. D. *J. Chem. Phys.* **1999**, *111*, 5267.
(45) Groot, R. D. *J. Chem. Phys.* **2003**, *118*, 11265.
(46) Gonzalez-Melchor, M.; Mayoral, E.; Velazquez, M. E.; Alejandre, J. *J. Chem. Phys.* **2006**, *125*, 224107.
(47) Ibergay, C.; Malfreyt, P.; Tildesley, D. J. *J. Chem. Theory Comput.* **2009**, *5*, 3245.

(48) Ibergay, C.; Malfreyt, P.; Tildesley, D. J. *J. Phys. Chem. B* **2010**, *114*, 7274.
(49) Goujon, F.; Malfreyt, P.; Tildesley, D. J. *J. Chem. Phys.* **2008**, *129*, 034902.
(50) Goujon, F.; Malfreyt, P.; Tildesley, D. J. *Macromolecules* **2009**, *42*, 4310.
(51) Pagonabarraga, I.; Frenkel, D. *J. Chem. Phys.* **2001**, *115*, 5015.
(52) Trofimov, S. Y.; Nies, E. L. F.; Michels, M. A. *J. Chem. Phys.* **2002**, *117*, 9383.
(53) Warren, P. B. *Phys. Rev. E* **2003**, *68*, 066702.
(54) Trofimov, S. Y.; Nies, E. L. F.; Michels, M. A. J. *J. Chem. Phys.* **2005**, *123*, 144102.
(55) Groot, R. D.; Madden, T. J. *J. Chem. Phys.* **1998**, *108*, 8713.
(56) Groot, R. D.; Madden, T. J.; Tildesley, D. J. *J. Chem. Phys.* **1999**, *110*, 9739.
(57) Prinsen, P.; Warren, P. B.; Michels, M. A. J. *Phys. Rev. Lett.* **2002**, *89*, 148302.
(58) Malfreyt, P.; Tildesley, D. J. *Langmuir* **2000**, *16*, 4732.
(59) Irfachsyad, D.; Tildesley, D. J.; Malfreyt, P. *Phys. Chem. Chem. Phys.* **2002**, *4*, 3008.
(60) Ibergay, C.; Malfreyt, P.; Tildesley, D. J. *Soft Matter* **2011**, *7*, 4900.
(61) Liew, C. C.; Mikami, M. *Chem. Phys. Lett.* **2003**, *368*, 346.
(62) Groot, R. D.; Rabone, K. L. *Biophys. J.* **2001**, *81*, 725.
(63) Ghoufi, A.; Malfreyt, P. *Phys. Rev. E* **2011**, *83*, 051601.
(64) Ghoufi, A.; Malfreyt, P. *J. Chem. Theory Comput.* **2012**, *8*, 787.
(65) Fetters, L. J.; Lohse, D. J.; Richter, D.; Witten, T. A.; Zirkel, A. *Macromolecules* **1994**, *27*, 4639.
(66) Smith, G. D.; Paul, W. *J. Phys. Chem. A* **1998**, *102*, 1200.
(67) Hoover, W. G. *Phys. Rev. A* **1985**, *31*, 1695.
(68) Espanol, P.; Warren, P. B. *Europhys. Lett.* **1995**, *30*, 191.
(69) Press, W. H.; Flannery, B. P.; Teukolsky, S. A.; Vetterling, W. T. *Numerical Recipes in C: The Art of Scientific Computing*; Cambridge University Press: New York, 1992.
(70) Goujon, F.; Ghoufi, A.; Malfreyt, P.; Tildesley, D. J. *Soft Matter* **2012**, *8*, 4635.
(71) Likhtman, A. E.; Sukumaran, S. K. *Macromolecules* **2010**, *43*, 3980.
(72) Seidel, C. *Macromolecules* **2003**, *36*, 2536.
(73) Likhtman, A. E.; Sukumaran, S. K.; Ramirez, J. *Macromolecules* **2007**, *40*, 6748.
(74) Lee, W. B.; Kremer, K. *Macromolecules* **2009**, *42*, 6270.
(75) Peters, G. H.; Tildesley, D. J. *Phys. Rev. E* **1996**, *54*, 5493.
(76) DiBenedetto, A. T. *J. Appl. Polym. Sci. A1* **1963**, *3*, 459.
(77) Tsolou, G.; Mavrantzas, V. G.; Theodorou, D. *Macromolecules* **2005**, *38*, 1478.
(78) Berendsen, H. J. C.; Postma, J. P. M.; van Gunsteren, W.; DiNola, A.; Haak, J. R. *J. Chem. Phys.* **1984**, *81*, 3684.
(79) Mattice, W. L.; Suter, U. W. *Conformational Theory of Large Molecules*; Wiley: New York, 1994.
(80) Rubinstein, M.; Colby, R. H. *Polymer Physics*; Oxford University Press: Oxford, 2003.
(81) Bennemann, C.; Paul, W.; Binder, K.; Dünweg, B. *Phys. Rev. E* **1998**, *57*, 843.
(82) de Gennes, P. G. *J. Chem. Phys.* **1971**, *55*, 572.
(83) Sukumaran, S. K.; Grest, G. S.; Kremer, K.; Everaers, R. *J. Polym. Sci., Part A: Polym. Phys.* **2005**, *43*, 917.
(84) Ramirez, J.; Sukumaran, S. K.; Vorselaars, B.; Likhtman, A. E. *J. Chem. Phys.* **2010**, *133*, 154103.
(85) Byutner, O.; Smith, G. S. *Macromolecules* **2002**, *35*, 3769.
(86) Liu, P.; Harder, E.; Berne, B. *J. Phys. Chem. B* **2005**, *109*, 2949.